High resolution infrared spectra of neopentane: Rovibrational analysis of bands at 8.3–6.4 μm

Adam Pastorek, Peter Bernath, Vincent Boudon

High Resolution Infrared Spectra of Neopentane: Rovibrational Analysis of Bands at 8.3-6.4 µm

Adam Pastorek[1,*], Peter Bernath[1], Vincent Boudon[2]

1 – Department of Chemistry and Biochemistry, Old Dominion University, Norfolk, Virginia 23529, United States of America

2 – Laboratoire Interdisciplinaire Carnot de Bourgogne, UMR 6303 CNRS – Université de Bourgogne, 9 Av. A. Savary, Dijon Cedex BP 47870, F-21078, France

** Corresponding author*

Abstract

High resolution (0.0014 cm^{-1}) infrared spectra of neopentane (2,2-dimethylpropane) have been recorded at 203 K at the Canadian Light Source. Spectra were recorded in the infrared (8.3-6.4 µm) with 8 m of optical path. Neopentane is a spherical top molecule with T_d (tetrahedral) symmetry. A low temperature is favorable for a detailed rotational analysis of its fundamental bands.

This study focuses on the analysis of 3 band systems of neopentane. The first system is a dyad consisting of a ν_{15} fundamental band and a $\nu_7 + \nu_{19}$ combination band located at 1472.5 and 1489 cm^{-1}, respectively. The second system is a ν_{16} fundamental band located at 1369.4 cm^{-1} with uncertain band origin. The third band system is a dyad of a ν_{17} fundamental and a $\nu_8 + \nu_{18}$ combination band. Only the ν_{17} fundamental band was analyzed in this last system due to the weaker intensity of the combination band. For all spectral simulations and calculations an 'XTDS' program based on tensorial formalism by the Dijon molecular spectroscopy group was used. A subprogram 'SPVIEW', paired with XTDS, was used for spectral assignment.

Keywords

Infrared spectroscopy, FTIR, neopentane, spherical top

Introduction

Neopentane (2,2-dimethylpropane) is a methane-like spherical top molecule with tetrahedral symmetry (T_d). Because of its compact structure and high symmetry, neopentane has a higher melting point and lower boiling point than its isomers (*n*-pentane, isopentane), being the only gaseous isomer at room temperature. Also, neopentane has a lower enthalpy of fusion than its isomers, as expected from its high symmetry.

Common hydrocarbons including various C_2-C_5 alkanes can be found globally in Earth's atmosphere[1] or for example in the atmosphere of Saturn[2] or its moon Titan. Titan's atmosphere may be a favorable environment for neopentane formation by photochemical and ion-chemical processes.[3] Eight other hydrocarbons have already been detected in Titan's atmosphere,[4] further suggesting the possibility of neopentane's presence. Allene was also recently observed in Titan's atmosphere[5] by use of high-resolution infrared spectroscopy, showing the importance of spectroscopy as an analytical tool for remote sensing of planetary atmospheres.

Neopentane has also been extensively studied in catalysis, mainly from the point of view of hydrogenolysis. Hydrogenolysis of neopentane was studied by application of various metal catalysts like Rh/Al_2O_3, Pt, Pd or Au-containing catalysts.[6–11] Such studies use neopentane in particular for the determination of the catalyst's activity (neopentane undergoes methane cracking in these hydrogenolysis reactions with very favorable and relatively easy measurement).

Regarding the spectroscopic facts, neopentane has only 7 infrared-active fundamental vibrational bands (those of T_2 symmetry): ν_{13}-ν_{19}. Some of the vibrational frequencies have already been published as early as in 1947.[12] Since that time there have been a number of publications on neopentane vibrations measured by IR and Raman spectroscopy[13–17] and even neutron scattering.[18]

Theoretical work consisting of *ab initio* calculations of the neopentane's fundamental modes of vibration by Mirkin and Krimm[19] (based on the previous force field calculations by Schachtschneider and Snyder)[20] has provided a set of recommended vibrational frequencies

based on experimental observations. Electron diffraction measurements of neopentane by Bartell *et al.*[21] have provided a reliable molecular structure.

It is a well-known that allowed fundamental bands of spherical top molecules have their upper rotational levels split into 3 components by first-order Coriolis interaction. In addition, tetrahedral symmetry molecules have no dipole moment in the ground state, so pure rotational spectra are forbidden (although they can appear very weakly from centrifugal distortion in the rotating molecule). These limitations put spherical tops like neopentane into a special category and represent a challenge for their study.

The first and simplest spherical top molecule, methane, has already been spectroscopically analyzed long time ago (e.g., by Moorhead[22] in 1932), but more complex spherical tops still need a more thorough analysis or have been analyzed recently – like germane[23] or adamantane.[24,25]

This article presents an extension to our previous research on neopentane infrared spectra,[26–28] analyzing a spectrum with high resolution observed at low temperature, which is favorable for the experimental observation of neopentane's fundamental vibrations. We provide a detailed analysis of the rovibrational spectra by use of a tensorial formalism – a useful tool for the analysis of spherical tops.

Experimental arrangement

The spectrum was recorded at the Canadian Light Source (CLS) facility at the far-infrared beamline with a Fourier transform infrared spectrometer using the infrared glower. Detailed experimental details are provided in our paper on infrared absorption cross sections[28] and the spectrum is available from MoLList[29] at https://bernath.uwaterloo.ca/molecularlists.php (*Neopentane_24.8mTorr_MCTNW_GAINB_8M_203.45K_F3_032722_11.23_MIR_0.001400_80 kHz_KBr_BEB_AVG290_B2.0*). Briefly, the sample was placed in a White cell with multiple reflections of a light beam, totaling a pathlength of 8 m. The optics were made from KBr, including the entry windows of the cell. Neopentane in the cell was cooled to a temperature of 203.45 K and had a pressure of 24.8 mTorr. A liquid nitrogen-cooled MCT (mercury cadmium telluride) detector was used. The unapodized spectral resolution was 0.0014 cm^{-1} and the spectra were recorded in

the range of 1100-1800 cm^{-1} set by a bandpass filter. 290 scans were accumulated to obtain a reasonably high signal-to-noise ratio. The aperture size was 1.15 mm.

A scheme of the experimental arrangement is shown in Figure 1.

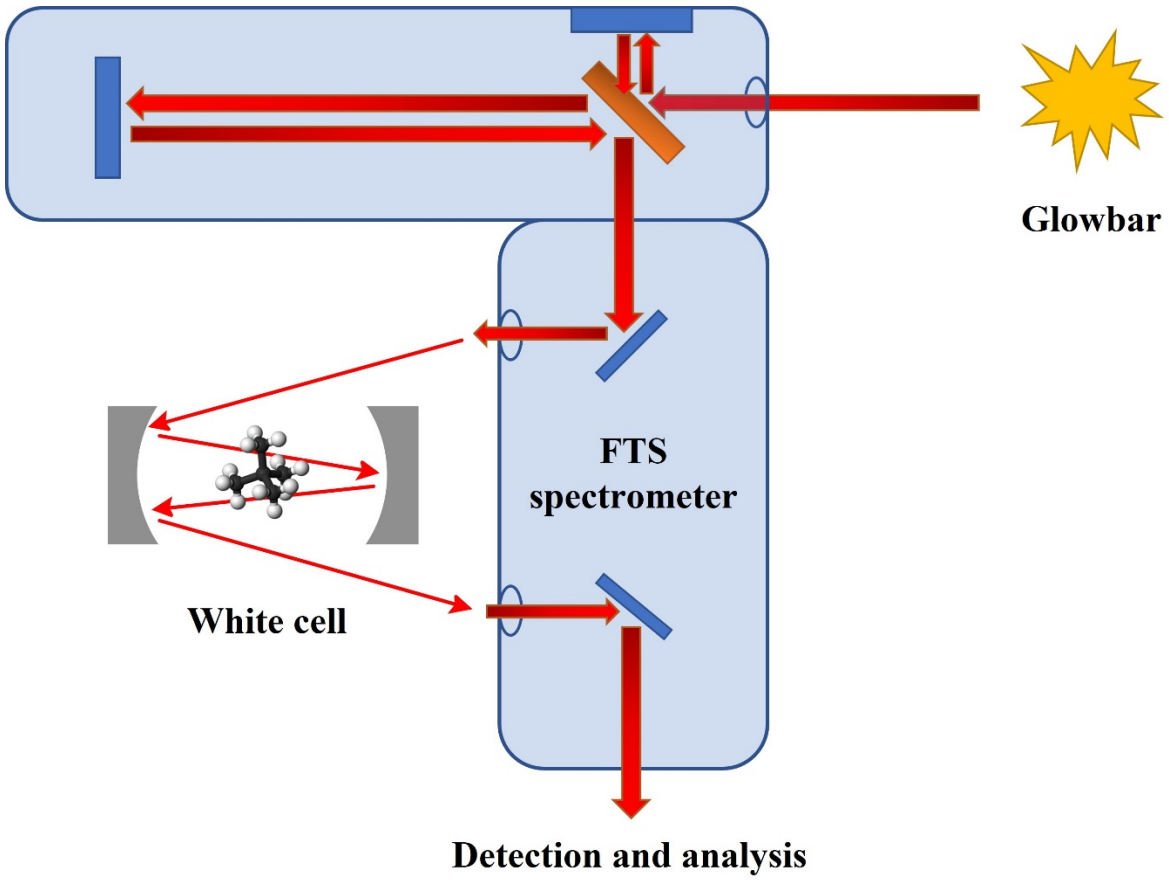

Figure 1: Experimental arrangement

Results and discussion

The overall spectrum of neopentane in the 1100-1800 cm^{-1} spectral range is depicted in Figure 2 below.

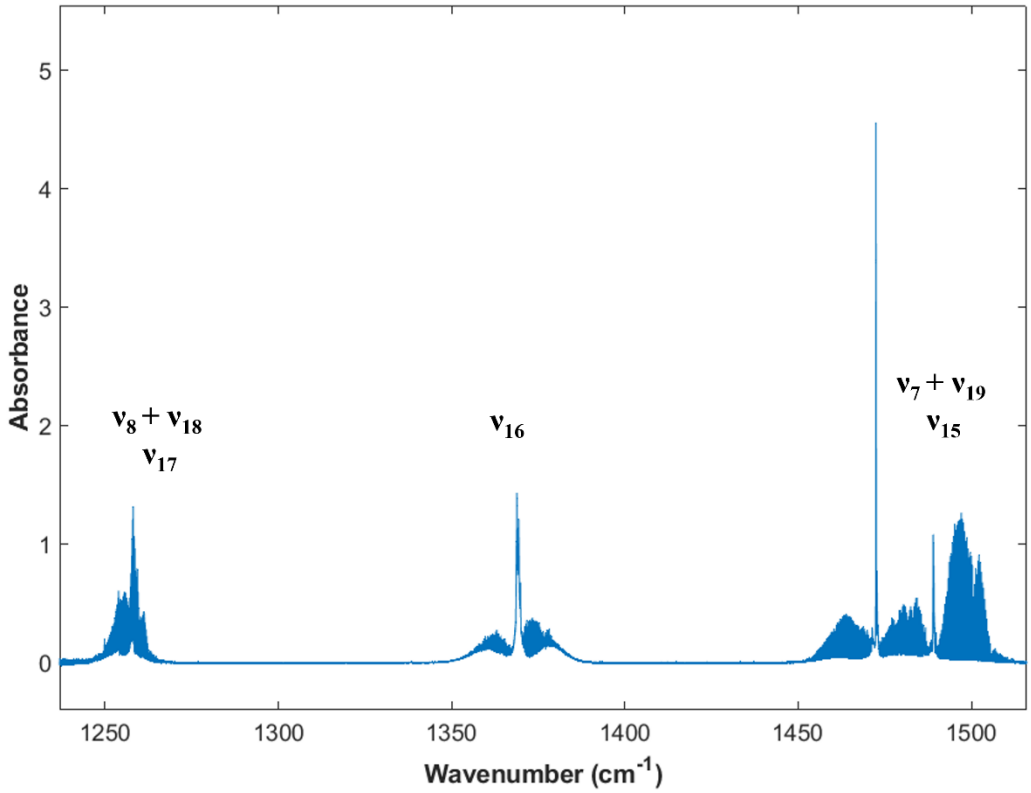

Figure 2: Overall absorbance spectrum of neopentane in the 1235-1525 cm^{-1} spectral range

As can be seen from Figure 2, neopentane has 3 band systems in the recorded spectral range. The rightmost system centered roughly around 1485 cm^{-1} is a dyad of a ν_{15} fundamental band and a $\nu_7 + \nu_{19}$ combination band. The middle band is a ν_{16} fundamental vibration band. Finally, the leftmost band system consists of a ν_{17} fundamental band and a $\nu_8 + \nu_{18}$ combination band, together forming another dyad.[26,28]

ν_{15} / $\nu_7 + \nu_{19}$ dyad

Focusing first on the rightmost band system in Figure 2; Figure 3 is an expanded view of the dyad.

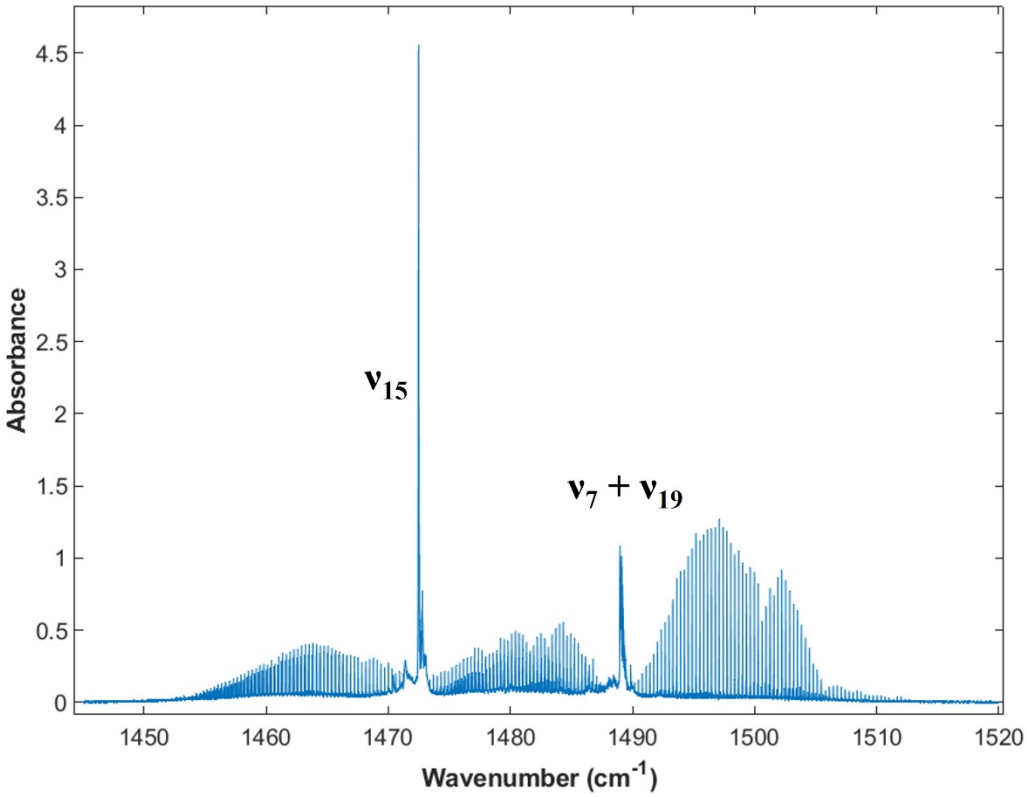

Figure 3: Expanded view of the ν_{15} / $\nu_7 + \nu_{19}$ dyad

The region between 1450-1470 cm^{-1} in Figure 3 contains only the ν_{15} fundamental vibration's P-branch and the region of 1490-1515 cm^{-1} contains only the R-branch of the $\nu_7 + \nu_{19}$ combination band. The middle region of 1474-1488 cm^{-1} contains both R-branch of the fundamental band and P-branch of the combination band, creating many overlaps and blending of lines. Additionally, one may notice a significant perturbation in the R-branch region of the combination band, centered around 1501 cm^{-1}. Cluster splittings are not present in this region. This contrasts with an extremely strong cluster splitting present in the P-branch region of the fundamental band (1450-1470 cm^{-1}), where one line can be split into 15 components at high J values.

This dyad has been assigned using the SPVIEW software and fitted using the XTDS program,[30] based on a tensorial formalism.[31] The dyad has been fitted as a whole, accounting for interactions between both bands, even though in the end no interactions were found. An expanded

view of the P-branch of the ν_{15} fundamental band together with the simulated model can be observed in Figure 4.

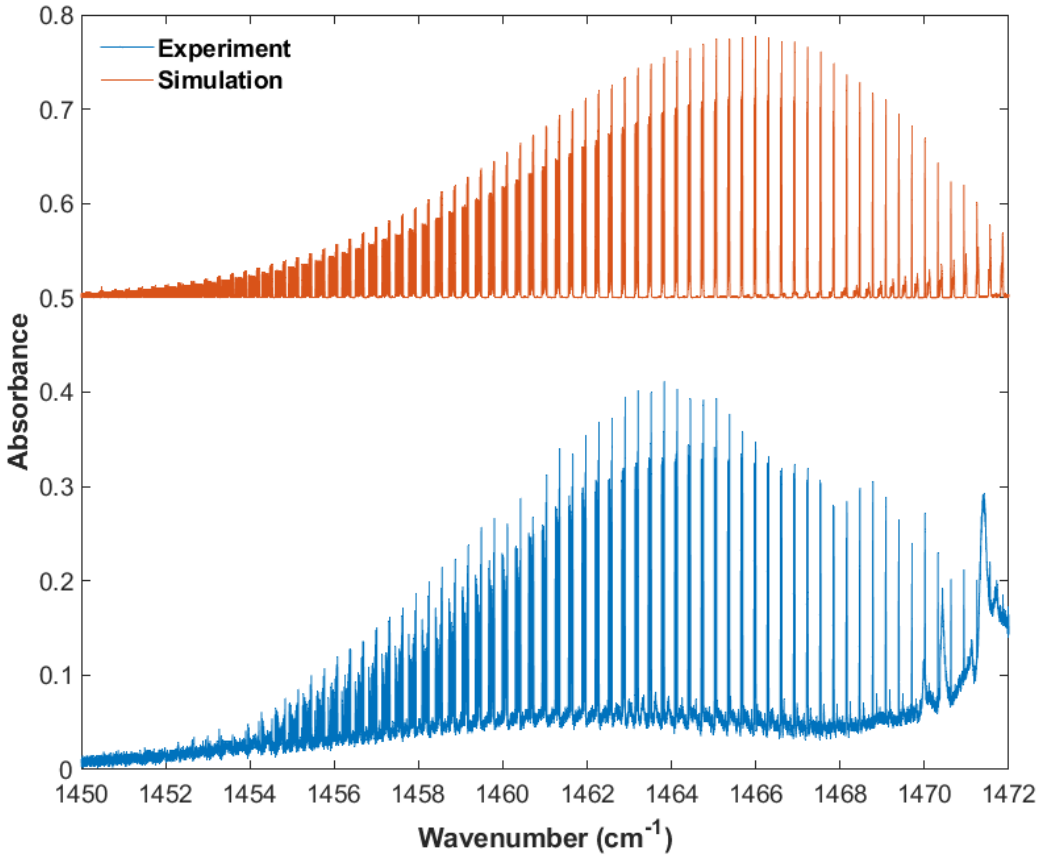

Figure 4: Expanded view of the P-branch of the ν_{15} fundamental band and the simulation

The simulation matches the experimental line positions well in the selected region of 1450-1472 cm^{-1}, although the transitions with low J-numbers show some deviations from the experimental spectrum as can be seen in Figure 5.

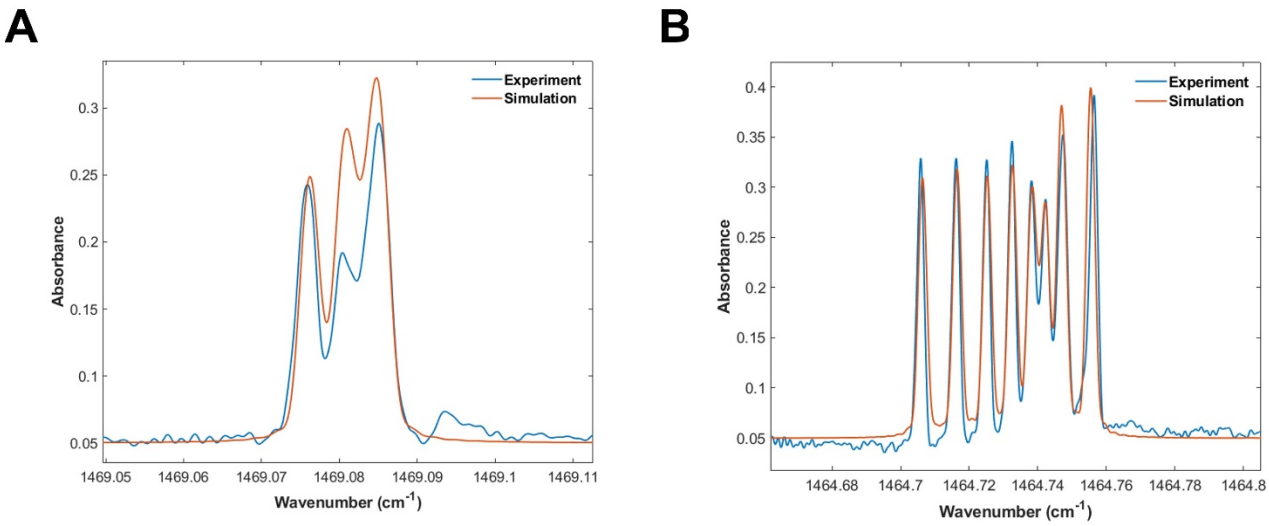

Figure 5: A – Cluster J′ = 10
B – Cluster J′ = 24

As can be seen in panel A of Figure 5, the fitted line shape is not ideal especially for this transition with relatively low J-number. On the other hand, the J′ = 24 transition is fitted almost ideally. An especially good fit can also be seen in transitions with high J-numbers, e. g. J′ = 42, which is depicted in Figure 6.

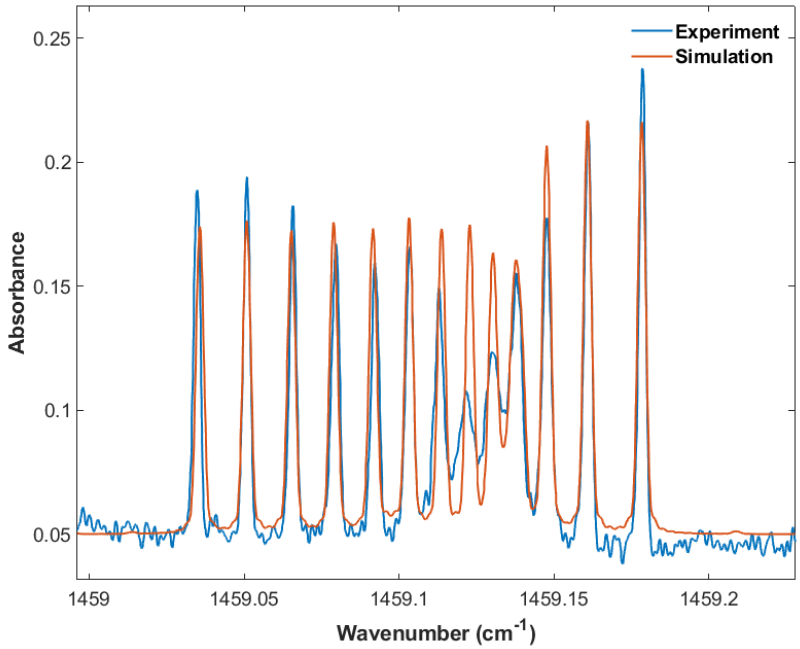

Figure 6: Cluster J′ = 42 of the ν_{15} P-branch

The R-branch of the $\nu_7 + \nu_{19}$ combination band is shown in Figure 7 together with the simulation.

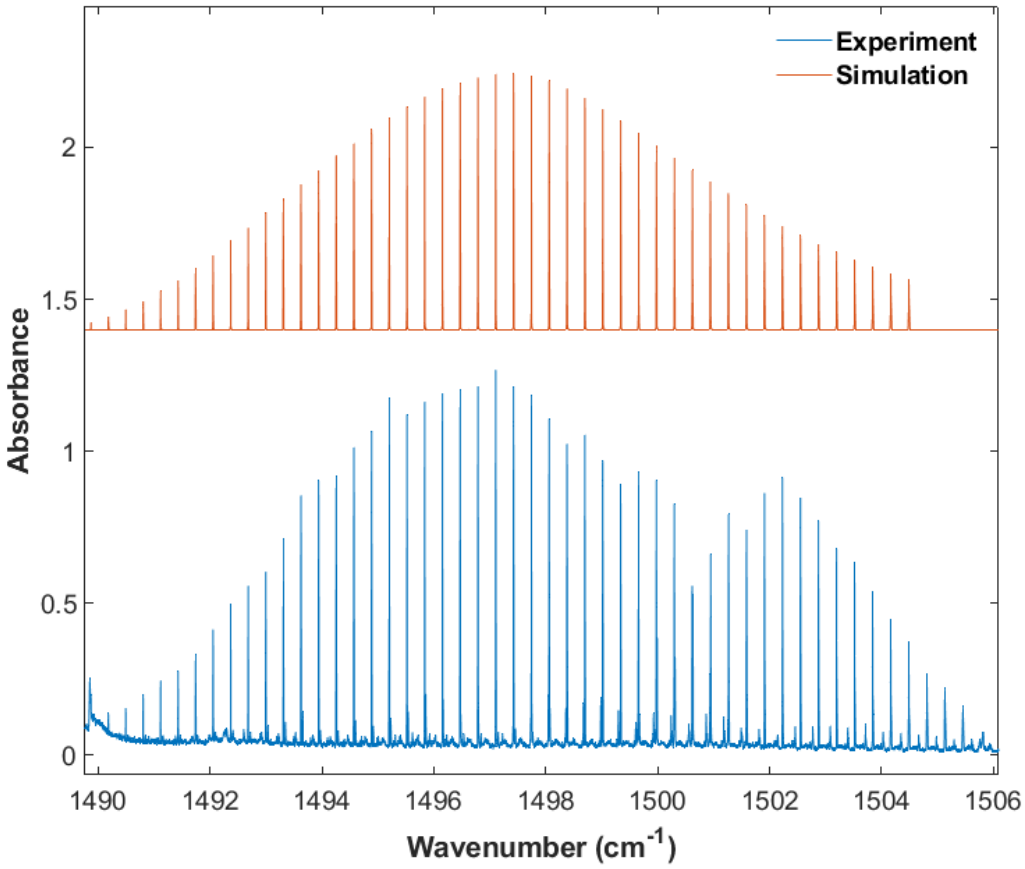

Figure 7: Expanded view of the R-branch of the $\nu_7 + \nu_{19}$ combination band and the simulation

Since the splitting in the R-branch in Figure 7 above is negligible, all lines in this spectral range are fitted with single line profiles with minimal deviation. The only exception is lines at highest J-numbers (around 1504 cm^{-1}, J ~ 50), which exhibit a shape deformation (see Figure 8 for a detailed view).

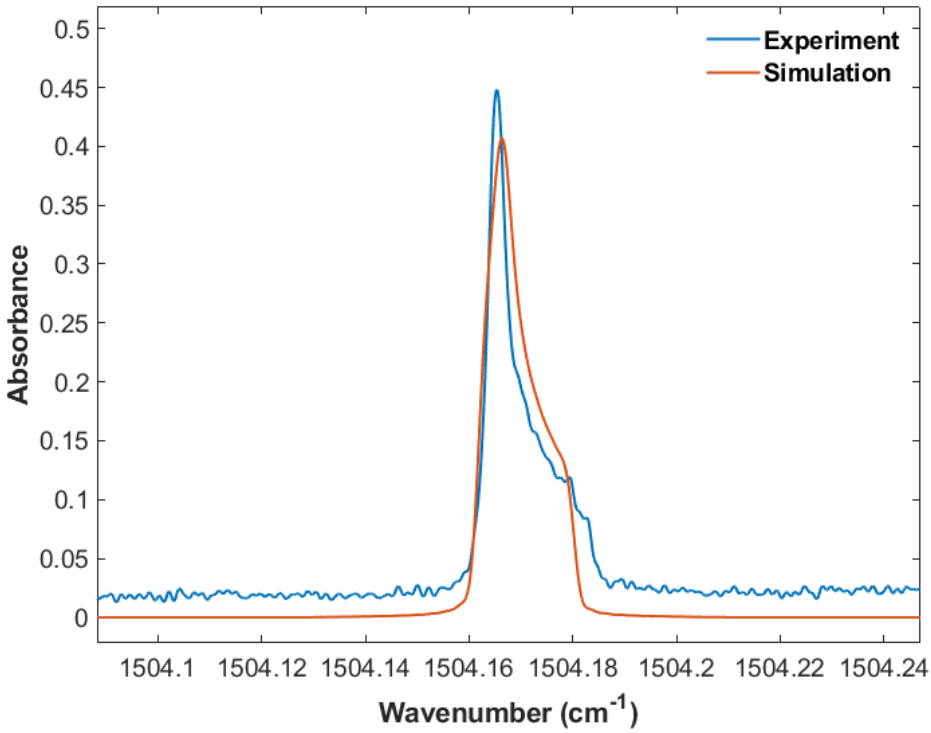

Figure 8: Detailed view of the J' = 48 R-branch line of the $\nu_7 + \nu_{19}$ combination band

The middle region of 1474-1488 cm^{-1} between the two distinguished Q-branches contains both R-branch of the fundamental band and P-branch of the combination band and therefore exhibits many overlaps. The overall spectrum of this region together with the simulation is shown in Figure 9.

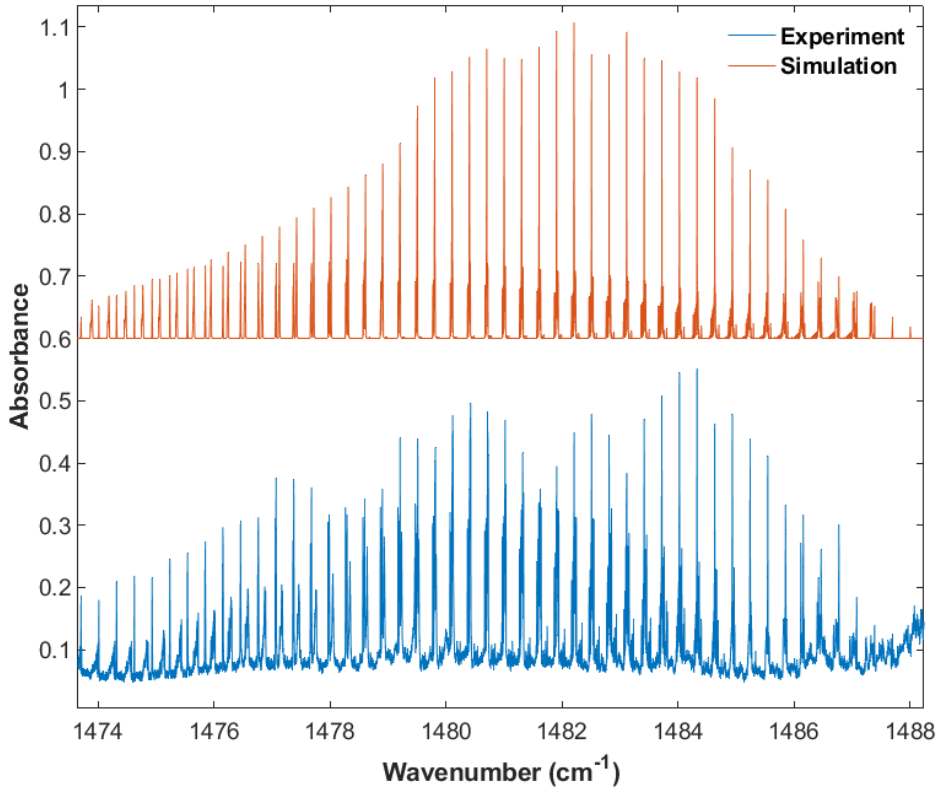

Figure 9: The middle region of the ν_{15} / $\nu_7 + \nu_{19}$ dyad

An expanded region around 1474 cm^{-1} can be seen in Figure 10.

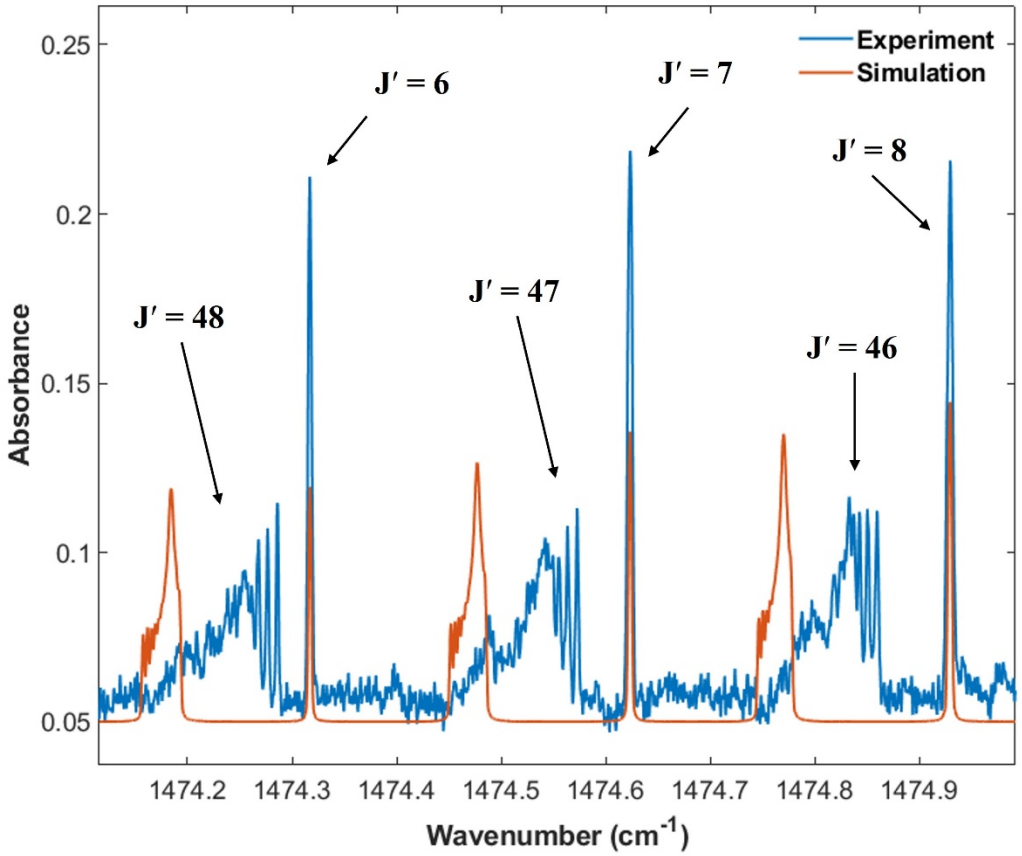

Figure 10: A detailed zoom of several lines around 1474 cm^{-1} region

As can be seen in Figure 10, R-branch lines of the ν_{15} fundamental band of neopentane (J' = 6, 7, 8) match the lines of the simulation well. On the other side, P-branch lines of the $\nu_7 + \nu_{19}$ combination band of higher J-numbers reside in this area as well (J' = 48, 47, 46), and they exhibit a cluster splitting hardly matched by the simulation. A more detailed analysis will be needed to account for the complex shape of these P-branch lines.

The situation changes on the other side of the middle region, towards the 1486 cm^{-1}. An expanded view of the lines present in this spectral region is depicted in Figure 11.

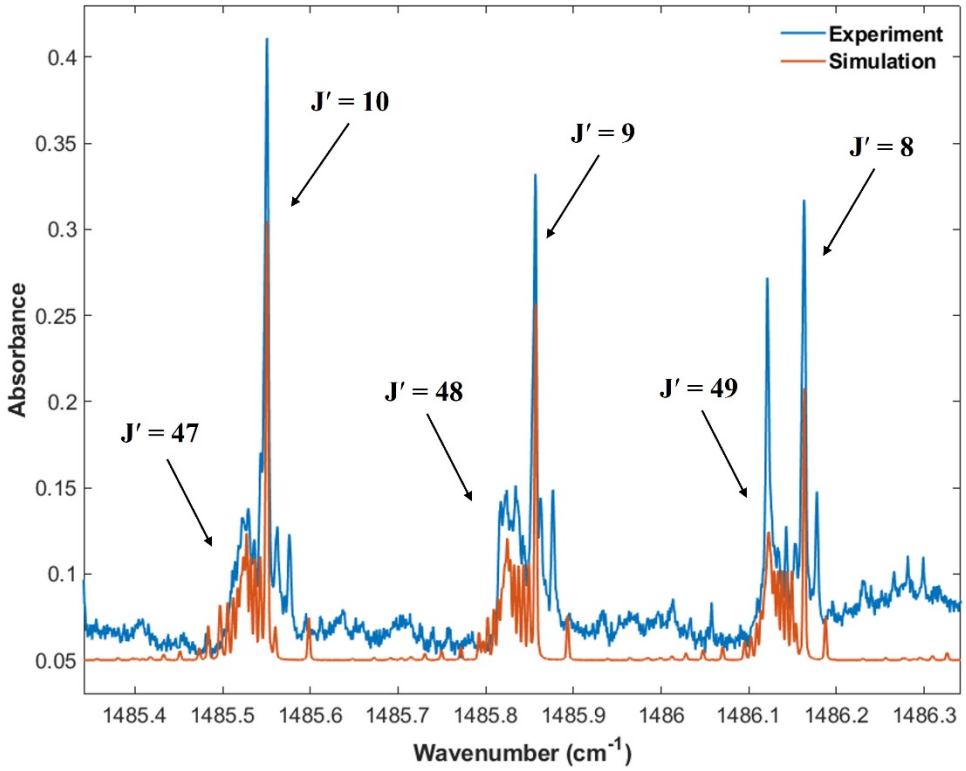

Figure 11: Expanded view of several lines in the 1486 cm^{-1} region

Figure 11 shows three P-branch lines of the $\nu_7 + \nu_{19}$ combination band (J′ = 10, 9, 8) that show no cluster splitting at these relatively low J-numbers. These lines overlap with heavily split high-J R-branch lines of the ν_{15} fundamental band. Whereas the relative position of the clusters is well simulated, the exact shape of clusters is not well simulated.

A newly calculated set of nuclear spin statistics was used to account for the intensity distribution between individual lines in clusters.

In short, we used the method developed by Berger (1977).[32] This leads to a nuclear spin representation $\Gamma_{SN} = 232A_1 + 136A_2 + 352E + 488T_1 + 520T_2$. In the case of neopentane, the only atoms with a non-zero nuclear spin are hydrogens (we do not consider possible ^{13}C carbon isotopes in this study) which are fermions (1/2 nuclear spin). As a consequence, the total wavefunction should change sign in any odd permutation of 2 hydrogen atoms and it is thus easy to show that it should have A_2 symmetry. Consequently, taking into account the two possible parities ($\tau = g$ or u)

of the rotational function, we find that the rovibrational (RV) part of the wavefunction should satisfy

$$\Gamma_{SN} = A_2 \otimes \Gamma_{RV(\tau)}$$

The result is that A_1, A_2, E, T_1 and T_2 rovibrational wavefunctions get spin statistical weights 368, 368, 704, 1008 and 1008, respectively. These weights are taken into account for all intensity calculations of the present paper.

A set of spectroscopic constants expressed in tensorial formalism used to simulate the ν_{15} / $\nu_7 + \nu_{19}$ dyad of neopentane is provided in Table 1.

Table 1: Effective Hamiltonian parameters for the ν_{15} / $\nu_7 + \nu_{19}$ dyad of neopentane

Ω (*K*, *nC*)	**{s} C_1**	**{s'} C_2**	**Value**	**Std. dev.**	**Std. notation**
$2(0,0A_1)$	A_1	A_1	0.1469*		B_0
$0(0,0A_1)$	ν_{19}, F_2	ν_{19}, F_2	418*		ν_{19}
$0(0,0A_1)$	ν_7, E	ν_7, E	1060*		ν_7
$0(0,0A_1)$	$\nu_7 + \nu_{19}, F_1$	$\nu_7 + \nu_{19}, F_1$	1480*		ν_{15} / $\nu_7 + \nu_{19}$
$0(0,0A_1)$	$\nu_7 + \nu_{19}, F_2$	$\nu_7 + \nu_{19}, F_2$	10.921424979	$1.498029\cdot10^{-4}$	
$1(1,0F_1)$	$\nu_7 + \nu_{19}, F_2$	$\nu_7 + \nu_{19}, F_2$	$-3.3576775998\cdot10^{-2}$	$2.138422\cdot10^{-5}$	$3\sqrt{2}\,B\zeta\,(\nu_7 + \nu_{19})$
$2(0,0A_1)$	$\nu_7 + \nu_{19}, F_2$	$\nu_7 + \nu_{19}, F_2$	$1.7643577015\cdot10^{-4}$	$8.633663\cdot10^{-7}$	$B(\nu_7 + \nu_{19}) - B_0$
$2(2,0E)$	$\nu_7 + \nu_{19}, F_2$	$\nu_7 + \nu_{19}, F_2$	$-5.6265105364\cdot10^{-6}$	$3.172111\cdot10^{-6}$	
$3(1,0F_1)$	$\nu_7 + \nu_{19}, F_2$	$\nu_7 + \nu_{19}, F_2$	$-1.7333216702\cdot10^{-7}$	$2.777244\cdot10^{-8}$	
$3(3,0F_1)$	$\nu_7 + \nu_{19}, F_2$	$\nu_7 + \nu_{19}, F_2$	$-1.2291569951\cdot10^{-7}$	$3.610460\cdot10^{-8}$	
$4(0,0A_1)$	$\nu_7 + \nu_{19}, F_2$	$\nu_7 + \nu_{19}, F_2$	$-3.5845125072\cdot10^{-9}$	$4.541950\cdot10^{-10}$	
$0(0,0A_1)$	ν_{15}, F_2	ν_{15}, F_2	1472.461453	$8.224813\cdot10^{-5}$	ν_{15}
$1(1,0F_1)$	ν_{15}, F_2	ν_{15}, F_2	$-2.9498681433\cdot10^{-2}$	$9.532905\cdot10^{-6}$	$3\sqrt{2}\,B\zeta\,(\nu_{15})$
$2(0,0A_1)$	ν_{15}, F_2	ν_{15}, F_2	$-5.4467762561\cdot10^{-5}$	$2.342549\cdot10^{-7}$	$B_{15} - B_0$
$2(2,0E)$	ν_{15}, F_2	ν_{15}, F_2	$-1.4466089767\cdot10^{-4}$	$2.536487\cdot10^{-7}$	$-(1/2)\alpha^{15}_{220} - 6\alpha^{15}_{224}$
$2(2,0F_2)$	ν_{15}, F_2	ν_{15}, F_2	$-6.1249332818\cdot10^{-6}$	$4.676303\cdot10^{-7}$	$-(3/4)\alpha^{15}_{220} + 6\alpha^{15}_{224}$
$3(1,0F_1)$	ν_{15}, F_2	ν_{15}, F_2	$-5.4148677843\cdot10^{-7}$	$5.847642\cdot10^{-9}$	$-(3(\sqrt{3})/4(\sqrt{2}))F^{15}_{110}$
$3(3,0F_1)$	ν_{15}, F_2	ν_{15}, F_2	$1.3470069695\cdot10^{-7}$	$5.316536\cdot10^{-9}$	$(3/\sqrt{5/2})F^{15}_{134}$
$4(0,0A_1)$	ν_{15}, F_2	ν_{15}, F_2	$4.7650948277\cdot10^{-9}$	$2.130733\cdot10^{-10}$	$-(D_{15} - D_0)$
$4(2,0E)$	ν_{15}, F_2	ν_{15}, F_2	$5.1923006126\cdot10^{-9}$	$2.943265\cdot10^{-10}$	$(\sqrt{3}/8)G^{15}_{220} + (3\sqrt{3}/2)G^{15}_{224}$
$4(4,0A_1)$	ν_{15}, F_2	ν_{15}, F_2	$1.9182699270\cdot10^{-9}$	$8.474930\cdot10^{-11}$	$(-3\sqrt{5/4}\sqrt{2})(D_{15f} - D_{0f})$
$4(4,0E)$	ν_{15}, F_2	ν_{15}, F_2	$2.4007164818\cdot10^{-9}$	$1.009408\cdot10^{-10}$	$(-3\sqrt{7/2})G^{15}_{244} + (\sqrt{21/2}\sqrt{22})G^{15}_{246}$

**Fixed values.*

Standard notation provided only when available. For the further explanation of used terms, see Boudon et al. (2004).[31]

ν_{16} fundamental band

The middle band in Figure 2 is a ν_{16} fundamental vibration band of neopentane. An expanded view of the fundamental band is in Figure 12.

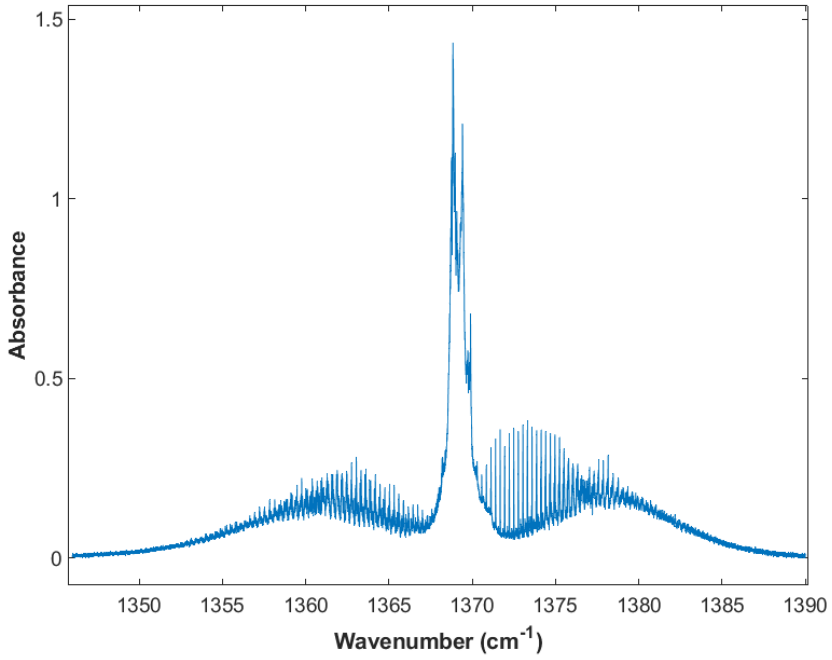

Figure 12: ν_{16} fundamental band of neopentane

At the first glance, the fundamental band in Figure 12 looks symmetric and therefore easy to fit, however the band is heavily perturbed and possibly overlapped. Figure 13 shows a closer look at the P-branch region of the ν_{16} band, together with the simulated spectrum.

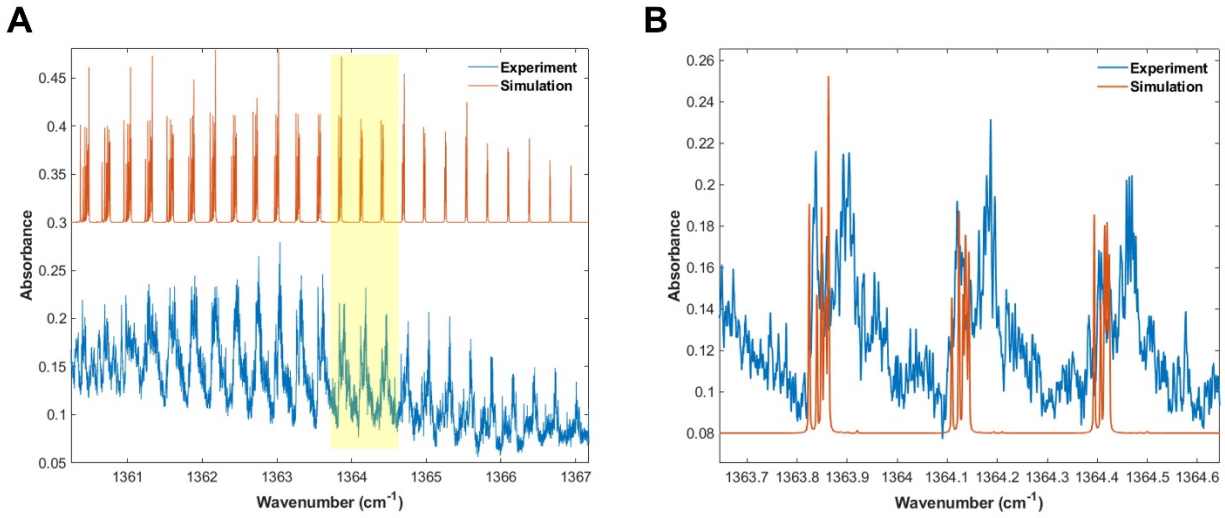

Figure 13: A – P-branch of the ν_{16} band of neopentane with simulation
B – Expanded view of several perturbed clusters in the P-branch

The panel A of Figure 13 shows the experimental spectrum of the P-branch of the ν_{16} band of neopentane together with the simulated model spectrum. The simulation might look acceptable but the expanded region around 1346 cm^{-1} depicted in panel B (highlighted in yellow in panel A) demonstrates the model is inadequate. A closer look at panel B of Figure 13 shows that the simulation only models the shape of the left branch of each cluster. This suggests the existence of perturbing band(s) which strongly affect the overall cluster shape. There could be a potential overlap of the ν_{16} band with either a $\nu_{18} + \nu_{19}$ or $\nu_{11} + \nu_{19}$ combination band (having 1342.2 and 1358 cm^{-1}, respectively); both are T_2 modes and therefore are IR-active. This would imply a positive anharmonicity, which is possible. Additionally, the possible existence of hot bands in the band system is also apparent in Figure 12.

Figure 14 below demonstrates an expanded view of the R-branch of the ν_{16} band of neopentane with the corresponding simulation.

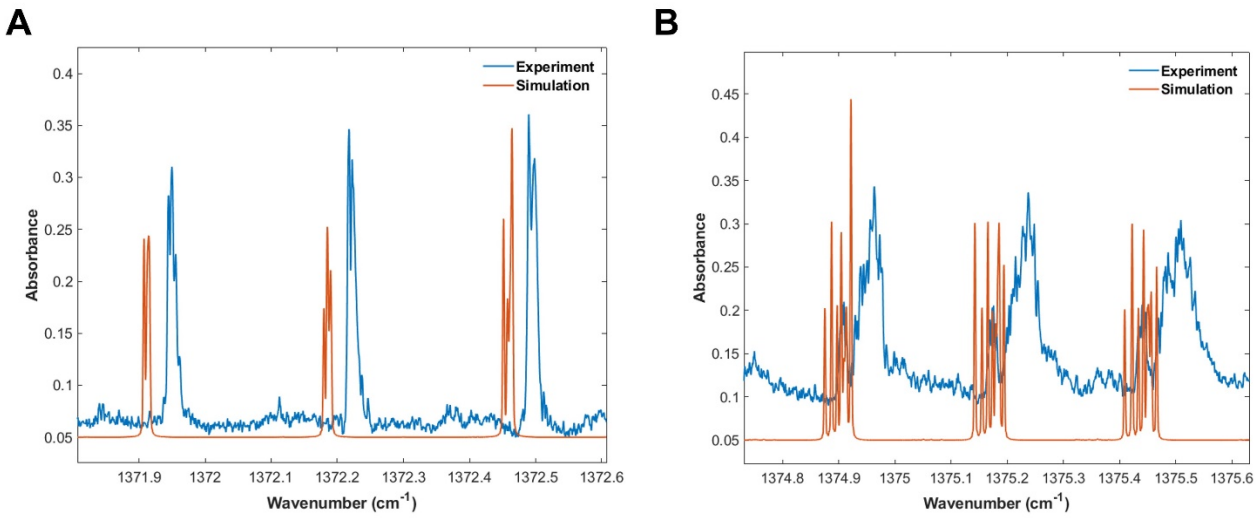

Figure 14: A – Lower J-number clusters of the R-branch of the ν_{16} band
B – Higher J-number clusters of the R-branch of the ν_{16} band

One may notice that whereas in panel B of Figure 14 the clusters are simulated only for the left half, in panel A the simulated clusters are simply shifted to the left since there are no additional features for the experimental J-clusters. Clearly, the perturbation becomes significant only for higher J-numbers.

The Q-branch of the ν_{16} band of neopentane has an unusual shape observed in detail in Figure 15.

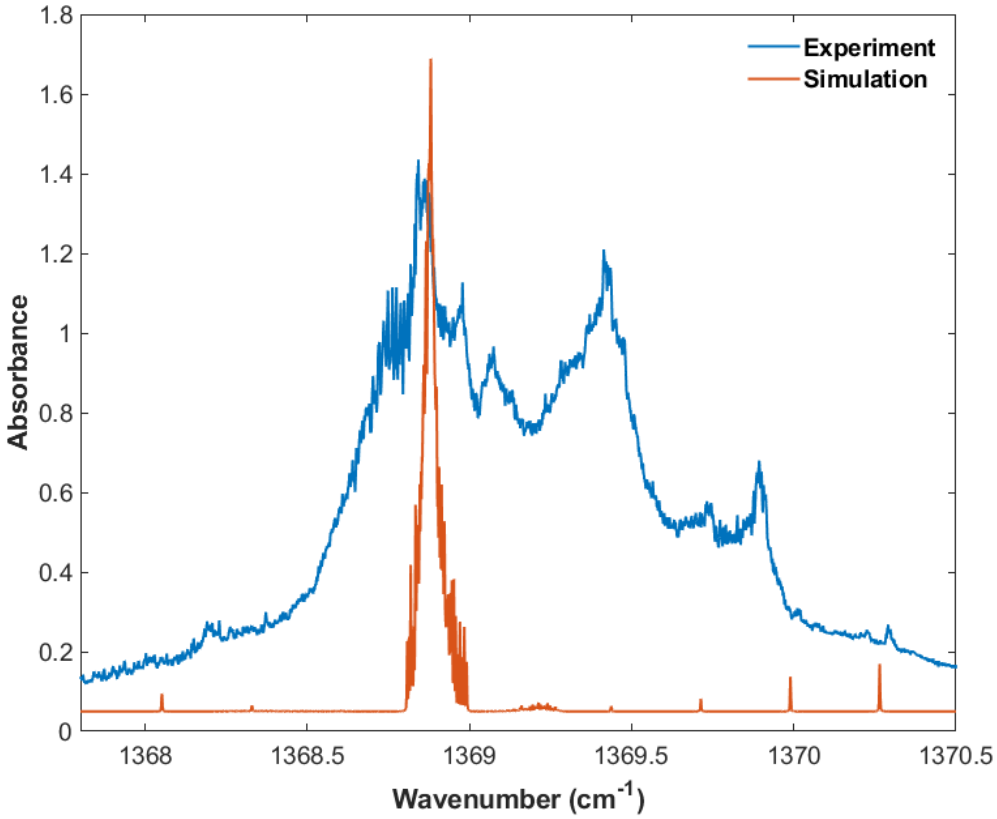

Figure 15: Expanded view of the Q-branch of the ν_{16} band of neopentane

Again, the shape of the Q-branch depicted in Figure 15 might be a result of an overlap with one of the combination bands; or the extra Q-branches could be hot bands. More detailed theoretical analysis is needed to determine the origin of the ν_{16} band perturbation.

Spectroscopic constants used for the simulation of the ν_{16} band of neopentane are given in Table 2. The ν_{16} band has been simulated as a standalone fundamental band with no interacting perturbers.

Table 2: Effective Hamiltonian parameters for the ν_{16} band of neopentane

Ω (*K*, *nC*)	**{s} C_1**	**{s'} C_2**	**Value**	**Std. dev.**	**Std. notation**
2(0,0A_1)	A_1	A_1	0.1469*		B_0
0(0,0A_1)	ν_{16}, F_2	ν_{16}, F_2	1368.9*		ν_{16}
1(1,0F_1)	ν_{16}, F_2	ν_{16}, F_2	$3.500 \cdot 10^{-2}$*		$3\sqrt{2}\, B\zeta\ (\nu_{16})$
2(0,0A_1)	ν_{16}, F_2	ν_{16}, F_2	$-1.000 \cdot 10^{-4}$*		$B_{16} - B_0$
2(2,0E)	ν_{16}, F_2	ν_{16}, F_2	$-2.000 \cdot 10^{-4}$*		$-(1/2)\alpha^{16}_{220} - 6\alpha^{16}_{224}$

**Fixed values.*

ν_{17} / $\nu_8 + \nu_{18}$ dyad

The leftmost band system in Figure 2 is a ν_{17} / $\nu_8 + \nu_{18}$ dyad of neopentane. Figure 16 depicts this dyad in detail.

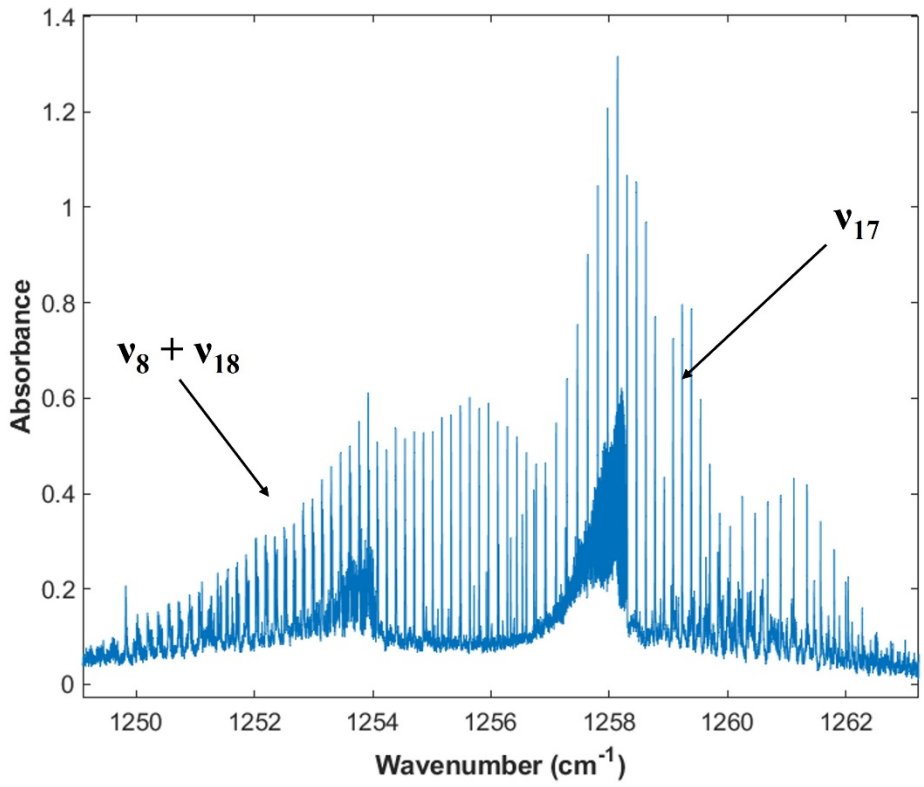

Figure 16: ν_{17} / $\nu_8 + \nu_{18}$ dyad of neopentane

The dyad depicted in Figure 16 has a strange appearance, suggesting strong perturbing effects in this region. The ν_{17} fundamental band, centered around 1257.6 cm^{-1} has its P-branch and R-branch lines shifted towards lower wavenumbers, as shown in Figure 17.

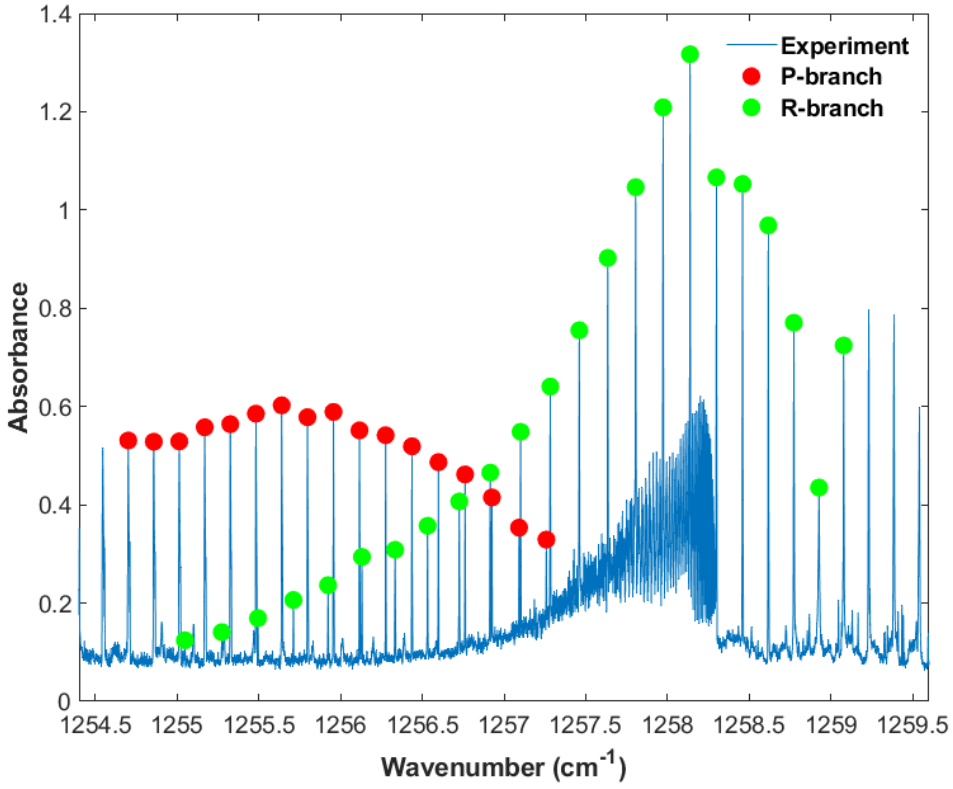

Figure 17: Extended view of the ν_{17} fundamental band of neopentane

R-branch lines of the ν_{17} fundamental band, shown in Figure 17, exhibit a clear decreasing spacing between two individual adjacent lines (decreasing line separation) with increasing J-number. This trend changes after the rightmost, green-marked, R-branch line in Figure 17 (located at 1259.07 cm^{-1}). R-branch lines with higher wavenumber exhibit the opposite trend of increasing line separation with increasing J-number. Additionally, there is a clear perturbation of the intensity pattern of R-branch lines at 1258.93 cm^{-1}. P-branch lines of the ν_{17} band up to $J' = 16$ follow the same trend of decreasing line separation with increasing J-number. The overall shape of the ν_{17} band of neopentane points to a mutual interaction between both components of the ν_{17} / $\nu_8 + \nu_{18}$ dyad.

The system must be fitted as an interacting dyad, which requires a knowledge of spectroscopic parameters of all fundamental vibrations involved in the band system (ν_{17}, ν_8, ν_{18}). Because such parameters are not known, the analysis of the whole dyad was not performed and only a test simulation of the dyad was produced. This simulation is depicted in Figure 18.

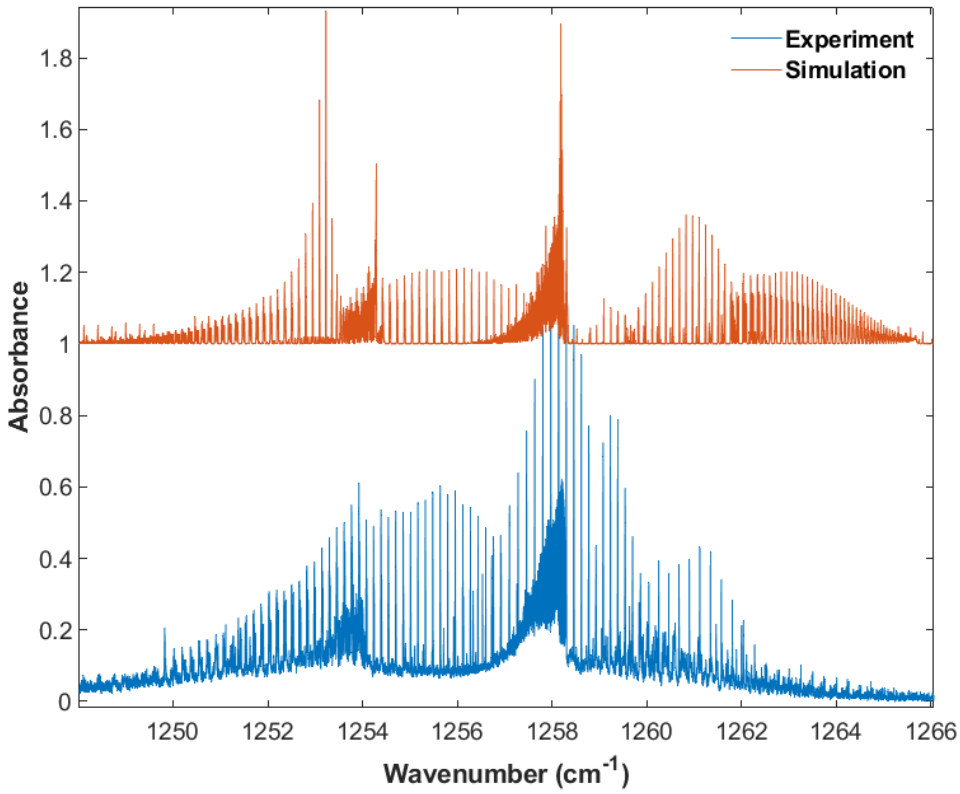

Figure 18: Test simulation of the ν_{17} / $\nu_8 + \nu_{18}$ dyad of neopentane

The simulation shown in Figure 18 was produced without a knowledge of Coriolis parameters, splitting parameters or rotational constant differences for ν_8 and ν_{18} bands. Nevertheless, this simulation attempt can potentially be used as a starting point for a more complete analysis of this dyad.

Spectroscopic constants used to generate the simulation depicted in Figure 18 can be seen in Table 3.

Table 3: Effective Hamiltonian parameters for the ν_{17} / $\nu_8 + \nu_{18}$ dyad of neopentane

Ω (*K*, *nC*)	**{s} C_1**	**{s'} C_2**	**Value**	**Std. dev.**	**Std. notation**
$2(0,0A_1)$	A_1	A_1	0.1469*		B_0
$0(0,0A_1)$	ν_8, E	ν_8, E	334*		ν_8
$0(0,0A_1)$	ν_{18}, F_2	ν_{18}, F_2	924.2*		ν_{18}
$1(1,0F_1)$	ν_{18}, F_2	ν_{18}, F_2	-0.600*		$3\sqrt{2}\,B\zeta\,(\nu_{18})$
$2(0,0A_1)$	ν_{18}, F_2	ν_{18}, F_2	$-3.000\cdot10^{-4}$*		$B_{18} - B_0$
$0(0,0A_1)$	ν_{17}, F_2	ν_{17}, F_2	1258.4619114	$2.793976\cdot10^{-4}$	ν_{17}
$1(1,0F_1)$	ν_{17}, F_2	ν_{17}, F_2	0.2971820342	$1.213896\cdot10^{-4}$	$3\sqrt{2}\,B\zeta\,(\nu_{17})$
$2(0,0A_1)$	ν_{17}, F_2	ν_{17}, F_2	$-2.9658825383\cdot10^{-4}$	$3.422935\cdot10^{-6}$	$B_{17} - B_0$
$2(2,0E)$	ν_{17}, F_2	ν_{17}, F_2	$3.6689446581\cdot10^{-5}$	$2.432653\cdot10^{-6}$	$-(1/2)\alpha^{17}_{220} - 6\alpha^{17}_{224}$
$3(1,0F_1)$	ν_{17}, F_2	ν_{17}, F_2	$-5.3951707802\cdot10^{-6}$	$5.390131\cdot10^{-8}$	$-(3(\sqrt{3})/4(\sqrt{2}))F^{17}_{110}$
$3(3,0F_1)$	ν_{17}, F_2	ν_{17}, F_2	$9.1607483033\cdot10^{-8}$	$2.719560\cdot10^{-8}$	$(3/\sqrt{5}/2)F^{17}_{134}$
$0(0,0A_1)$	F_2	F_2	-0.200*		
$0(0,0A_1)$	F_1	F_1	-4.000*		
$0(0,0A_1)$	F_2	F_2	-4.000*		

**Fixed values.*

Table 4 summarizes the symmetry of all analyzed bands of neopentane for informative purposes.

Table 4: Summary of symmetry for all analyzed bands of neopentane

Band	**Symmetry**
ν_7	E
ν_8	E
ν_{15}	F_2
ν_{16}	F_2
ν_{17}	F_2
ν_{18}	F_2
ν_{19}	F_2
$\nu_7 + \nu_{19}$	F_2
$\nu_8 + \nu_{18}$	F_2

Conclusion

Three band systems of neopentane in the 8.3-6.4 μm spectral range have been analyzed using a low temperature sample and high spectral resolution spectrum.

The first band system, a ν_{15} / $\nu_7 + \nu_{19}$ dyad, was analyzed in detail and a set of spectroscopic constants leading to a successful simulation is provided. The simulation matches the experimental spectrum well with the exception of P-branch lines of the $\nu_7 + \nu_{19}$ combination band for higher J-values.

The second band system, the ν_{16} fundamental vibration, was also analyzed and another set of spectroscopic constants was produced. However, in this case it must be noted that further theoretical analysis is needed. The provided simulation should only be used as a starting point for a reanalysis.

The last band system, a ν_{17} / $\nu_8 + \nu_{18}$ dyad, was not analyzed in detail and shows a heavily perturbed ν_{17} fundamental band. The simulation and spectroscopic constants provided are only a first step for a more detailed theoretical analysis.

Acknowledgement

The NASA Outer Planets Research and Planetary Data Archiving and Restoration Tools program (PDART) provided funding (80NSSC19K0417). Part of the research described in this paper was performed at the Canadian Light Source, a national research facility of the University of Saskatchewan, which is supported by the Canada Foundation for Innovation (CFI), the Natural Sciences and Engineering Research Council (NSERC), the National Research Council (NRC), the Canadian Institutes of Health Research (CIHR), the Government of Saskatchewan, and the University of Saskatchewan. PB acknowledges RB for productive discussion.

Authors' declaration

Authors declare no conflicts of interest.

References

[1] Pozzer A, Pollmann J, Taraborrelli D, Jöckel P, Helmig D, Tans P, et al. Observed and simulated global distribution and budget of atmospheric C 2-C5 alkanes. Atmos Chem Phys 2010;10:4403–22. https://doi.org/10.5194/acp-10-4403-2010.

[2] Moses JI, Bézard B, Lellouch E, Gladstone GR, Feuchtgruber H, Allen M. Photochemistry of Saturn's Atmosphere: I. Hydrocarbon Chemistry and Comparisons with ISO Observations. Icarus 2000;143:244–98. https://doi.org/10.1006/icar.1999.6270.

[3] Dobrijevic M, Loison JC, Hue V, Cavalié T, Hickson KM. 1D photochemical model of the ionosphere and the stratosphere of Neptune. Icarus 2020;335:113375. https://doi.org/10.1016/j.icarus.2019.07.009.

[4] Hörst SM. Titan's atmosphere and climate. J Geophys Res Planets 2017;122:432–82. https://doi.org/10.1002/2016JE005240.

[5] Lombardo NA, Nixon CA, Greathouse TK, Bézard B, Jolly A, Vinatier S, et al. Detection of Propadiene on Titan. Astrophys J 2019;881:L33. https://doi.org/10.3847/2041-8213/ab3860.

[6] Yao H, Shelef M. Hydrogenolysis of neopentane and n-pentane over a Rh/$gamma;-Al2O3 catalyst. J Catal 1979;56:12–20. https://doi.org/10.1016/0021-9517(79)90083-6.

[7] Karpinski Z, Larsson R. On the isokinetic effect of neopentane hydrogenolysis over metal catalysts. J Catal 1997;168:532–7. https://doi.org/10.1006/jcat.1997.1657.

[8] Karpinski Z, Butt JB, Sachtler WMH. Reaction of neopentane with hydrogen over Pd/SiO2. J Catal 1989;119:521–4. https://doi.org/10.1016/0021-9517(89)90181-4.

[9] Boudart M, Ptak LD. Reactions of neopentane on transition metals. J Catal 1970;16:90–6. https://doi.org/10.1016/0021-9517(70)90199-5.

[10] Foger K, Anderson JR. Skeletal reactions of neopentane over supported platinum-gold catalysts. J Catal 1980;61:140–5. https://doi.org/10.1016/0021-9517(80)90349-8.

[11] Rooney JJ. The mechanism of hydrogenolysis of neopentane on platinum catalysts. J Catal

1979;58:334–5. https://doi.org/10.1016/0021-9517(79)90272-0.

[12] Young CW, Koehler JS, McKinney DS, Young CW. Infrared Absorption Spectra of Tetramethyl Compounds. J Am Chem Soc 1947;69:1410–5. https://doi.org/10.1021/ja01198a050.

[13] Rank DH, Saksena BD, Shull ER. Vibrational spectra of carbon and silicon tetramethyl and their monodeutero derivatives. Discuss Faraday Soc 1950;9:187–96. https://doi.org/10.1039/DF9500900187.

[14] Shull ER, Oakwood TS, Rank DH. Infrared and Raman Spectra of Tetramethylmethane- d 12. J Chem Phys 1953;21:2024–9. https://doi.org/10.1063/1.1698736.

[15] Murata H, Shimizu K. Normal frequencies of tetramethylmethane. J Chem Phys 1957;27:599–600. https://doi.org/10.1063/1.1743788.

[16] Sportouch S, Lacoste C, Gaufrés R. Spectres Raman du néopentane et du tétraméthylsilane à l'état gazeux. J Mol Struct 1971;9:119–27. https://doi.org/10.1016/0022-2860(71)85012-3.

[17] Weiss S, Leroi GE. Infrared spectra and internal rotation in propane, isobutane and neopentane. Spectrochim Acta Part A Mol Spectrosc 1969;25:1759–66. https://doi.org/10.1016/0584-8539(69)80204-7.

[18] Jobic H, Sportouch S, Renouprez A. Neutron inelastic scattering spectrum and valence force field for neopentane. J Mol Spectrosc 1983;99:47–55. https://doi.org/10.1016/0022-2852(83)90291-6.

[19] Mirkin NG, Krimm S. Ab initio analysis of the vibrational spectra of conformers of some branched alkanes. J Mol Struct 2000;550–551:67–91. https://doi.org/10.1016/S0022-2860(00)00513-5.

[20] Schachtschneider JH, Snyder RG. Vibrational analysis of the n-paraffins—II. Normal co-ordinate calculations. Spectrochim Acta - Part A Mol Spectrosc 1989;45:307–11. https://doi.org/10.1016/S0584-8539(89)80281-8.

[21] Bartell LS, Bradford WF. Molecular structures of neopentane and di-tert-butylmethane by

vapor-phase electron diffraction. J Mol Struct 1977;37:113–26. https://doi.org/10.1016/0022-2860(77)87011-7.

[22] Moorhead JG. The Near Infrared Absorption Spectrum of Methane. Phys Rev 1932;39:83–8. https://doi.org/10.1103/PhysRev.39.83.

[23] Richard C, Boudon V, Rizopoulos A, Vander Auwera J, Kwabia Tchana F. Line positions and intensities for the ν2/ν4 bands of 5 isotopologues of germane near 11.5 μm. J Quant Spectrosc Radiat Transf 2021;260. https://doi.org/10.1016/j.jqsrt.2020.107474.

[24] Pirali O, Boudon V, Oomens J, Vervloet M. Rotationally resolved infrared spectroscopy of adamantane. J Chem Phys 2012;136. https://doi.org/10.1063/1.3666853.

[25] Pirali O, Boudon V. Synchrotron-based Fourier transform spectra of the ν23 and ν24 IR bands of hexamethylenetetramine C6N4H12. J Mol Spectrosc 2015;315:37–40. https://doi.org/10.1016/j.jms.2015.02.004.

[26] Bernath PF, Sibert EL, Dulick M. Neopentane Vibrations: High Resolution Spectra and Anharmonic Calculations. J Phys Chem A 2020;124:3438–44. https://doi.org/10.1021/acs.jpca.0c01723.

[27] Bernath P, Dodangodage R, Dulick M, Zhao J, Billinghurst B. Absorption cross sections for neopentane broadened by nitrogen in the 3.3 μm region. J Quant Spectrosc Radiat Transf 2020;251:1–5. https://doi.org/10.1016/j.jqsrt.2020.107034.

[28] Bernath P, Sibert EL, LaBelle K, Zhao J, Billinghurst B. Absorption cross sections and local mode analysis for neopentane. J Quant Spectrosc Radiat Transf 2022;293:108390. https://doi.org/10.1016/j.jqsrt.2022.108390.

[29] Bernath PF. MoLLIST: Molecular Line Lists, Intensities and Spectra. J Quant Spectrosc Radiat Transf 2020;240. https://doi.org/10.1016/j.jqsrt.2019.106687.

[30] Wenger C, Boudon V, Rotger M, Sanzharov M, Champion JP. XTDS and SPVIEW: Graphical tools for the analysis and simulation of high-resolution molecular spectra. J Mol Spectrosc 2008;251:102–13. https://doi.org/10.1016/j.jms.2008.01.011.

[31] Boudon V, Champion JP, Gabard T, Loëte M, Michelot F, Pierre G, et al. Symmetry-

adapted tensorial formalism to model rovibrational and rovibronic spectra of molecules pertaining to various point groups. J Mol Spectrosc 2004;228:620–34. https://doi.org/10.1016/j.jms.2004.02.022.

[32] Berger H. Classification of energy levels for polyatomic molecules. J Phys 1977;38:1371–5. https://doi.org/10.1051/jphys:0197700380110137100.